Nanomechanical Stability of Laterally Heterogeneous Films of Corrosion Inhibitor Molecules Obtained by Microcontact Printing on Au Model Substrates

Nanomechanical stability of laterally heterogeneous films of corrosion inhibitor molecules obtained by microcontact printing on Au model substrates

Andrea Valencia Ramirez[a,b], Gilles Bonneux[a,b], Andreas Terfort[c], Patricia Losada-Pérez[d], Frank Uwe Renner[a,b*]

[a] Institute for Materials Research, Hasselt University, 3590 Diepenbeek, Belgium

[b] IMEC vzw, Division IMOMEC, 3590 Diepenbeek, Belgium

[c] Institute of Inorganic and Analytical Chemistry, Goethe-University, 60438 Frankfurt am Main, Germany

[d] Experimental Soft Matter and Thermal Physics Laboratory, Université Libre de Bruxelles (ULB), 1050 Brussels, Belgium

*Email: frank.renner@uhasselt.be

Abstract

Self-assembled monolayers of corrosion inhibitors of the mercaptobenzimidazole family, SH-BimH, SH-BimH-5NH_2 and SH-BimH-5OMe, were formed on template-stripped ultraflat Au surfaces using microcontact printing, and subsequently analyzed using X-ray photoelectron spectroscopy (XPS), atomic force microscopy (AFM), and force spectroscopy (AFM-FS) using a quantitative imaging mode (QI). Printing of all used inhibitor molecules resulted in clear patterns and in slightly more compact films compared to immersion. The stability of the monolayers is further probed by AFM force spectroscopy. Adhesion values of laterally heterogeneous inhibitor-modified surfaces compared to bare Au surfaces, nonpatterned areas, and fully covered surfaces are analyzed and discussed. Microcontact printing confers a superior nanomechanical stability to imidazole-modified films of the printed surface patches as compared to homogeneously covered surfaces by immersion into the inhibitor solution.

Introduction

Surface functionalization of materials using self-assembled monolayers (SAMs) has been of wide interest for various applications due to their ability to spontaneously form highly compact and ordered monolayers onto the surfaces of solids (Figure 1a). SAMs can be used for biotechnology, microelectronics, and (more recently) corrosion inhibition[1–5]. Imidazole and mercapto-containing molecules have been demonstrated to be very good candidates for corrosion inhibitors on metals[5,6]. In terms of fundamental research, a number of surface science studies report the corrosion efficiency of homogeneously covered pure Cu surfaces, by both, experimental and theoretical approaches[5–10].

For the basic study of SAMs, mostly Au surfaces have been used and, as adsorbates, mainly linear alkanethiols have been used, with other more complex molecules being reported[11–13]. Au surfaces have been widely used due to their inert behavior at room temperature, ease of preparation, and availability, for example, as template-stripped ultraflat substrates (Figure 1b). Au thus provides a suitable reference system for the study of organic monolayer film formation and in particular of more complex (hybrid) corrosion inhibitor films.

The understanding of corrosion at the nanoscale and of the detailed mechanisms involved are still a matter of discussion due to the complexity of real materials, which involves the actual surface state, the eventual presence of various defects and impurities,[14] and the surrounding environment. Moreover, for studies at the atomic, molecular and nanoscale levels, in particular, experimentally challenging localized phenomena play a key role to understand and eventually prevent the early stages of corrosion[15–19].

We have previously introduced an approach to study corrosion inhibition at the nanoscale and localized level using a microcontact-printing (μ-cp) process. Using alkanethiols molecular boundaries were created in a controlled way[20,21]. For such well-controlled complex alkanethiol-modified alloy surfaces we could earlier show that initial localized dealloying corrosion is triggered at the created boundaries between two areas of different alkanethiols. Printing by μ-cp is a useful and low-cost approach, and works well for very flat substrates (Figure 1c). During the μ-cp process the organic molecules in solution are first deposited onto an elastomeric stamp (usually polydimethylsiloxane, PDMS), which, after removal of excess of solution, is subsequently placed onto the substrate to create patches of monolayers

following the topography on the stamp. This method has allowed to obtain high-resolution patterns on large areas as well as hybrid surfaces[22,23]. A full surface coverage including well-controlled patch-boundaries (single or double patterns), can be formed as a result of a final backfilling with the same or an additional type of molecules[24]. The adsorption behavior of mercaptobenzimidazole molecules on a reference system such as ultraflat Au surfaces has been barely investigated[25,26].

FS can be employed as a technique to evaluate the molecular film-substrate interactions at a nanoscale level[27] and to probe the stability of films. The stability of corrosion inhibitor films on metals and alloys, both on the general film-substrate level and the sites localized around molecular-level defects such as domain or patch boundaries, can be related to corrosion efficiency[27]. The literature reports the study of nanomechanical properties of alkanethiols adsorbed onto Au surfaces using FS,[28–31] but it has, to the best of our knowledge, not been the case for laterally structured heterogeneous surfaces formed by µ-cp and, in particular, with more bulky organosulfur molecules, which have shown a great potential as corrosion inhibitors.

Here we analyze model Au systems containing patterned layers formed from bulky organic molecules considered as corrosion inhibitors by surface characterization with X-ray photoelectron spectroscopy (XPS), atomic force microscopy (AFM), and AFM-force spectroscopy (AFM-FS) using a quantitative imaging (QI) mode. The nanomechanical properties of corrosion inhibitor films have been rarely investigated and, in addition, µ-cp has not yet been reported for the organosulfur compounds presented here. We assess the effect of heterogeneity in the nanomechanical properties of the modified surfaces combined with the study of their surface composition, their molecule-surface bonding, as well as the order or disorder of laterally structured complex SAMs. We also compare these results with homogeneously covered Au surfaces.

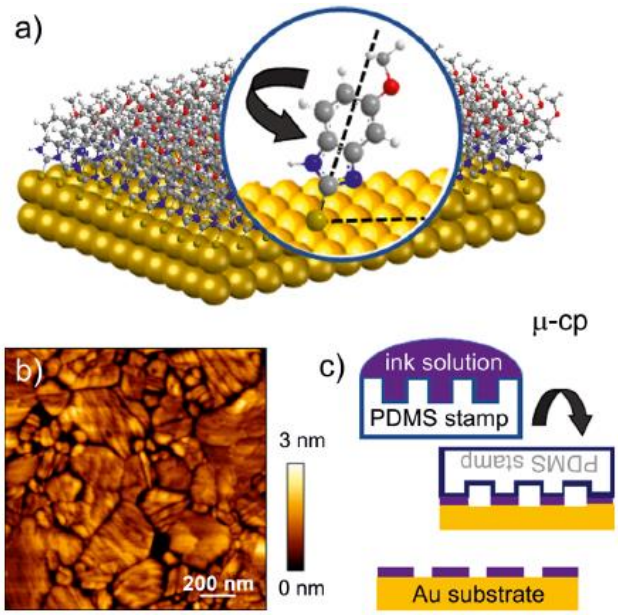

Figure 1. (a) Artistic view of molecule assembly on a metallic surface, (b) AFM image of ultraflat Au substrate surface (1.5 x 1.5 μm^2) and (c) schematic process of μ-cp.

Experimental methods

Chemicals used

2-Mercapto benzimidazole, 5-amino-2-mercapto benzimidazole, and 5-methoxy-2-mercapto benzimidazole (SH-BimH, SH-BimH-5NH_2, and SH-BimH-5OMe, respectively) were obtained from Fluorochem. Figure. 2 shows the chemical structure of each of these molecules. Absolute ethanol (99.5%) was provided by VWR. All chemicals were used without any further treatment. Thiol solutions of 1 mM concentration in ethanol were prepared and ultrasonicated in an ultrasonic bath purchased from VWR.

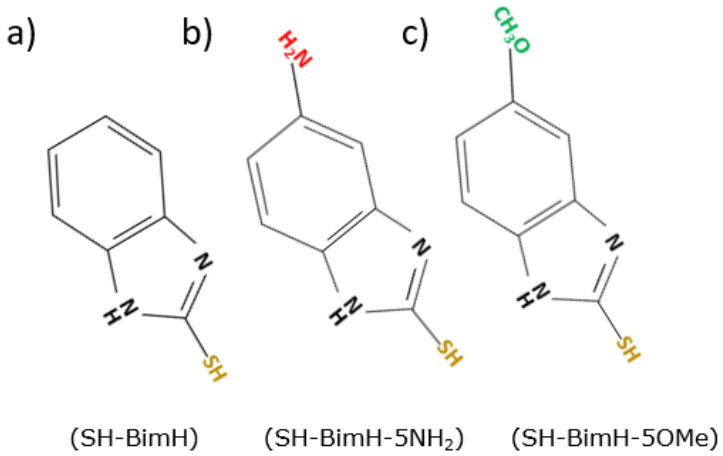

Figure 2. Schematic of chemical structures for (a) 2-mercaptobenzimidazole, (b) 5-amino-2-mercaptobenzimidazole, (c) 5-methoxy-2-mercaptobenzimidazole. The thiolate structure is shown.

Au substrates

Ultraflat polycrystalline Au substrates consisting of glass chips coated with a 100 nm Au layer, which are template-stripped from a silicon wafer, were purchased from Platypus Technologies. The substrates were used without any further treatment. The average roughness of each substrate is 0.3 nm according to manufacturer data sheet. The localized roughness varies in a range of 0.5 ± 0.4 nm as obtained from AFM imaging.

Formation of inhibitor films

Polydimethylsiloxane (PDMS) stamps with individual squared patches of ~4 x 4 µm were used to form the patterned surfaces. Prior to patterning, the stamps were rinsed and ultrasonicated in pure ethanol for 10 minutes and dried under N_2 gas. Droplets of the thiol containing solution were placed on the stamp for 30 seconds approximately, and the excess of solution was removed using N_2 gas. The stamp was subsequently placed onto the Au substrate and finally peeled off after 30 s (Figure 1c). In addition to the films formed by µ-cp, and for comparison purposes, three ultraflat Au surfaces were immersed overnight in each molecule solution, yielding homogeneously SAM-modified surfaces. After immersion, these samples were rinsed with ethanol and dried using N_2 gas.

AFM characterization

The AFM characterization of samples was carried out prior to performing FS measurements, using a JPK-Bruker NanoWizard 3 AFM in alternating current (AC) mode in air and silicon ACTA tips from AppNano with a cantilever length 125 µm, spring constant 40 N/m, and a resonance frequency of ~300 kHz.

Force Spectroscopy Measurements (AFM-FS)

For quantitative imaging (called QI mode for JPK-Bruker) measurements, SHOCONGG Au-coated Si tips from AppNano with a cantilever length of 225 µm and a resonance frequency of ~50 kHz were used. In the QI mode, fast force curves are recorded sequentially for each pixel. Prior to QI measurements, the tips were thoroughly cleaned with 95% H_2SO_4, DI water, and ethanol and dried with N_2. The cantilevers were also calibrated on clean ultraflat Au using the thermal noise method, obtaining spring constant values ranging from 0.07 to 0.1 N/m, which correspond to the spring constant specified for these particular cantilevers. Force curves were collected on patterned samples immersed in DI water in a selected surface area of 6 x 6 μm^2 to guarantee the acquisition of force curves in both patterned and non-patterned regions, applying a set point force of maximum 3 nN and setting both approach and retract speed of 3 µm/s. Force curves were also collected on bare ultraflat Au surfaces and on homogeneously covered surfaces for comparison purposes.

X-ray Photoelectron Spectroscopy characterization

XPS spectra were recorded using a Scienta Omicron setup with a monochromatic Al K-alpha X-ray source (1486.6 eV). Photoelectrons were detected via a hemispherical analyzer (EW4000). Pass energies of 200 and 100 eV were applied for the survey spectra and core level spectra, respectively. Measurements were recorded at pressures below 10^{-8} mbar. The Au 4f 7/2 core-level energy (84 eV) was used for the energy calibration of the spectra. Survey analysis and peak fitting of the core level spectra was performed using the CasaXPS software.

Results and discussion

Single printing

At the beginning of the experiments, prior to any patterning process, the commercial ultraflat bare Au surfaces were characterized by AFM in air using AC mode. Figure 1b provides an example of the surface topography of the bare Au samples, where different grain sizes as well as a number of growth-holes at the grain boundaries are observed. A broader view of the bare ultraflat Au sample, and the respective cross section profile are available in Figure S1. The μ-cp process for corrosion inhibitor films has been previously introduced[20,21,24]. For surface modification, we used 2-mercapto-benzimidazole, 5-amino-2-mercapto-benzimidazole, and 5-methoxy-2-mercapto-benzimidazole (SH-BimH, SH-BimH-5NH_2 and SH-BimH-5OMe), respectively, which are all frequently used in the context of corrosion inhibition, in particular for Cu and Cu alloys[6–9,27,32,33]. After μ-cp, the presence of printed patterns on ultraflat Au surfaces for the respective molecules is confirmed by AFM, as observed in Figure 3a-c. The formed patterns are clearly distinguishable and display a well-defined topography, similar to microcontact printed surfaces with alkanethiols reported elsewhere.[20,21,24]

Figure 3d-f shows the corresponding cross-sectional profiles, and the dashed lines indicate an ideal assembly of the molecules present in each patch. Each of the applied molecular patches shows a difference in height. The lowest thickness corresponds to the film formed by SH-BimH (Figure 3d), whereas the SH-BimH-5NH_2 (Figure 3e) and SH-BimH-5OMe (Figure 3f) films display a larger thickness. The molecular length of these molecules is of about 1 nm,[6] whereas DFT calculations suggest that molecules bind with the S atom and one of the N atoms to form an inclination that leads to a film of about 0.6 nm thickness.[5]

The irregularities in height observed in the obtained images and profiles, specifically in the sections corresponding to the thicker, patterned areas, may be attributed not only to the grain boundaries, the defects of the Au substrate such as the growth holes observed in Figure 1b, and the slight variations of local roughness but also to irregularities such as domain boundaries in the organic monolayers itself. In the lower thickness, presumed bare Au areas, possible individual, eventually flat-lying molecules could also be present. As a side remark, we have also observed in blank prints without impregnated molecules a small transfer of

(short) silicone chains from the PDMS stamp, in line with reports in the literature[34–40]. The corresponding AFM images, where "blank" patches are visible only by a small change in the phase signal but not in height images, are shown in Figure S1.

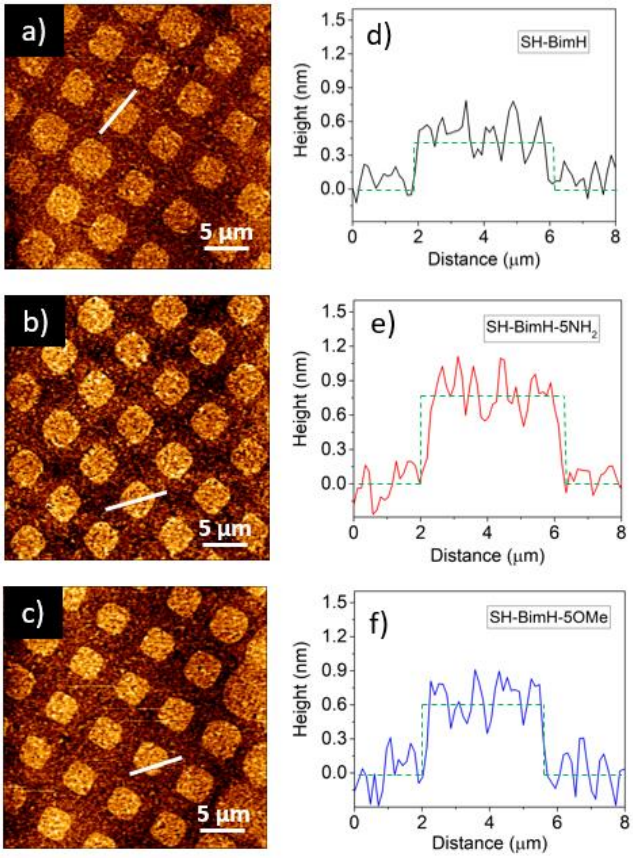

Figure 3. AFM images of single µ-cp patterns corresponding to (a) SH-BimH (b) SH-BimH-5NH_2, and (c) SH-BimH-5OMe and (d-f) their respective height cross section profiles. Color scale ranges from 0 to 3 nm.

XPS measurements

XPS measurements were recorded in order to analyze the surface composition of the print-modified samples as well as the fully covered ultraflat Au substrates, which were obtained by the direct immersion of bare substrates. Figure 4 shows the survey spectra corresponding to a printed ultraflat Au substrate with SH-BimH-5OMe as an example (the result is very similar for the other surfaces; the survey spectra of the remaining molecules are shown in Figure S2). Peaks corresponding to C and O are identified at energies ~285 and 530 eV respectively and, additionally, at energies of ~1020 and 1040 eV, two small peaks

corresponding to Zn were identified in all the shown spectra. The small Zn peaks were also observed in the bare ultraflat Au surface and the signal is very low (Figure S3). We therefore attribute these peaks to possible minor contaminations during the manufacturing process of the substrates. Moreover, since the Scofield factor of Zn 2p is high and the observed intensity is low, the quantification of elements indicates that the evidenced content of Zn is also very low, ranging between 0.3 and 1 at% on both bare and inhibitor-modified surfaces, which means there is no significant influence on the majority of the surface. It is also remarkable that the height of these Zn peaks diminishes in inhibitor-modified substrates, indicating the modification on top of the complete initial surface in both printed and fully covered samples.

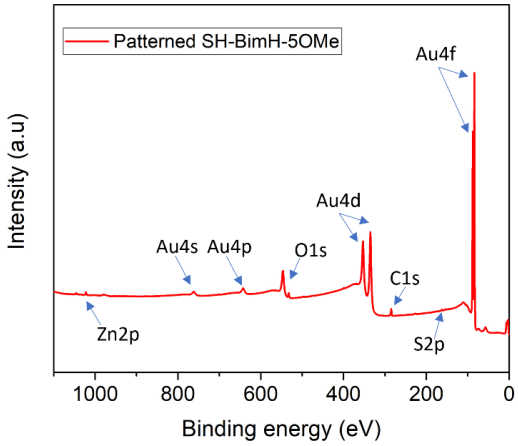

Figure 4. XPS spectra of a selected sample, µ-cp patterned ultraflat Au substrate with SH-BimH-5OMe.

In the case of patterned samples, it has been observed, as in the literature, the presence of Si is attributed to a limited transfer of (short) silicone chains from the PDMS stamp[34–40]. Nevertheless, the contribution of Si in the studied samples was minor also in the XPS signal; thus, no detrimental effect was observed in the SAM films.

High-resolution core-level spectra for S 2p of fully covered (Figure 5a-c) as well as printed (Figure 5d-f) Au substrates with the respective molecules are presented in Figure 5. The non-filled black circles form the measured spectrum, and the black solid line represents the envelope obtained after the respective fitting process. Each S 2p signal is fitted using three components which correspond to

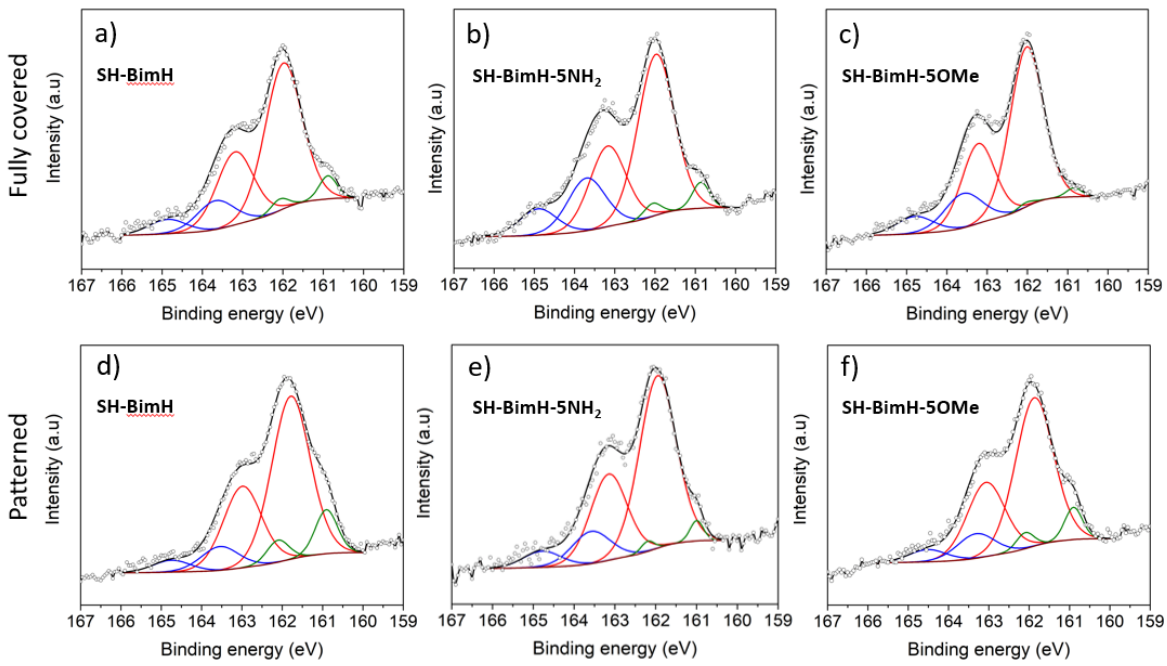

Figure 5. High-resolution peak in the S 2p region (a-c) of ultraflat Au substrates immersed overnight in respective solutions and (d-f) μ-cp patterned ultraflat Au substrates. Black solid line represents the fitting; open black circles correspond to measurement; red and blue solid lines correspond to bound and unbound thiol, respectively, and green solid lines are attributed to the possible reaction of S with Zn.

the bound sulfur (red solid lines), the unbound sulfur (blue solid lines) spectra typically observed in thiol molecules[41] and a small third component (green solid lines) of Zn-S attributed, as discussed above, to a possible reaction between Zn and S[42,43]. The Zn-S component is visible as the small shoulder observed in all the spectra at an energy of ~ 161 eV. This shoulder in the measured peaks is, in general, more noticeable in Figure 5d-f, corresponding to the patterned Au substrates, in line with an only partially covered surface. The relative intensity on the print-modified surfaces of the bound S peaks is also clearly higher compared to the nonbound signal in all cases, indicating the larger predominance of a covalent S-Au adsorption pointing to a better ordered film. Thus, the lower intensity of the unbound sulfur peak observed on the printed surfaces in comparison to the fully covered surfaces suggests more compact layers after the μ-cp process.

Force spectroscopy measurements using Quantitative Imaging mode (QI)

After confirming the presence of thiol films on the substrates in the topography images obtained in the AC mode AFM in air, each sample was measured using QI mode in deionized water. As mentioned in the experimental section, the main advantage of the QI mode is obtaining a force curve on each pixel of a chosen area. From the force curves data, different information can be derived such as an adhesion image or setpoint height image. Figure 6a,b presents examples of typical force curves obtained during the measurements in both bare ultraflat Au surface and µ-cp-modified Au surface.

In Figure 6a, the approach curve (black) remains at a force equal to zero until the tip-surface distance is ~2 nm where a pull-in force occurs due to the attractive interaction between the Au-coated tip and the Au surface, before the repulsive force takes over up to the hard wall repulsion when the tip contacts the Au surface. During the retract curve (red) at a very short distance, the tip experiences a pull-off force, the so called adhesion force which is expected to be high, since the Au-Au interaction requires a higher force to retract the tip towards its initial position[44]. Figure 6b shows a force curve where an adhesion peak in the retract curve is also visible for the µ-cp-modified Au surface with SH-BimH-5NH_2. Yet, the adhesion is significantly smaller in comparison to the adhesion force on bare Au. In addition, a second minimum in the retract curve at a distance of ~5 nm is visible. This behavior of the retracting curve has been explained previously as 'fishing' of molecules[27], where during the retract process the retract force between the tip and the sample is strong enough to pick a molecule or a group of molecules from the surface.

Adhesion and (un)folding of biomolecules is the most common field where this phenomenon is studied using the so called single-molecule force spectroscopy method, where the aim is to measure the interaction forces between biomolecules and different material interfaces as well as their nanomechanical properties[45–47]. This method frequently includes the functionalization of AFM tips, which consists in the conjugation of biomolecules onto the tip. Nevertheless, this is not the case of the present study since the tip was not modified. For a more detailed force curve data analysis in our study, 100 curves were randomly selected from non-patterned areas and 100 curves from a patterned region, thus 200 curves in total for each sample.

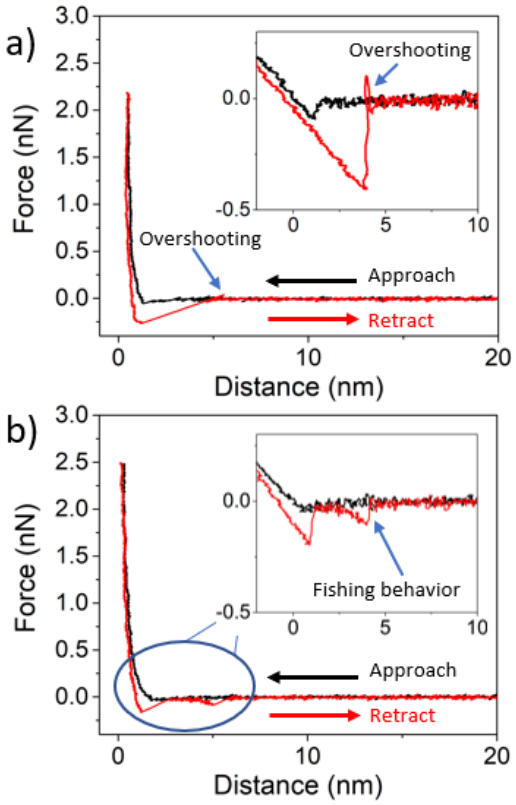

Figure 6. FS curves after correction for hard walls. (a) FS curve measured in bare ultraflat Au. The inset is a zoom image of the adhesion range of a raw force curve. An overshooting is also observed in the retract curve, corresponding to a higher oscillation amplitude and (b) FS curve measured in a µ-cp modified Au surface with SH-BimH-5NH_2. The inset plot shows the zoom image of the adhesion and fishing peaks observed in the raw retract curve.

Figures 7a-c shows the derived QI setpoint-height image of each inhibitor patterned surface at a resolution of 256 x 256 pixels. The dashed lines enclose the patch selected for measurements on each case for an easier view. In the same figure, white dots are observed, which may correspond to agglomeration of inhibitor molecules. The µ-cp patches are not clearly visible on the QI setpoint height images as they show the height information corresponding to the maximum force applied (setpoint), i.e., the layer forming the patch is compressed and is possibly penetrated by the tip; thus, the substrate is imaged.

As the force curves are taken on each pixel of the image, a value of adhesion is also obtained, from which it is possible to have an adhesion image as displayed in Figure 7d-f, which

presents the adhesion channel images obtained during the QI process. In all images, the presence of each microcontact-printed patch is clearly noticed and the adhesion values in the printed area are smaller compared to the nonpatterned areas, where a maximum adhesion of 407 pN is observed on the color scale. Further adhesion analysis will be discussed later.

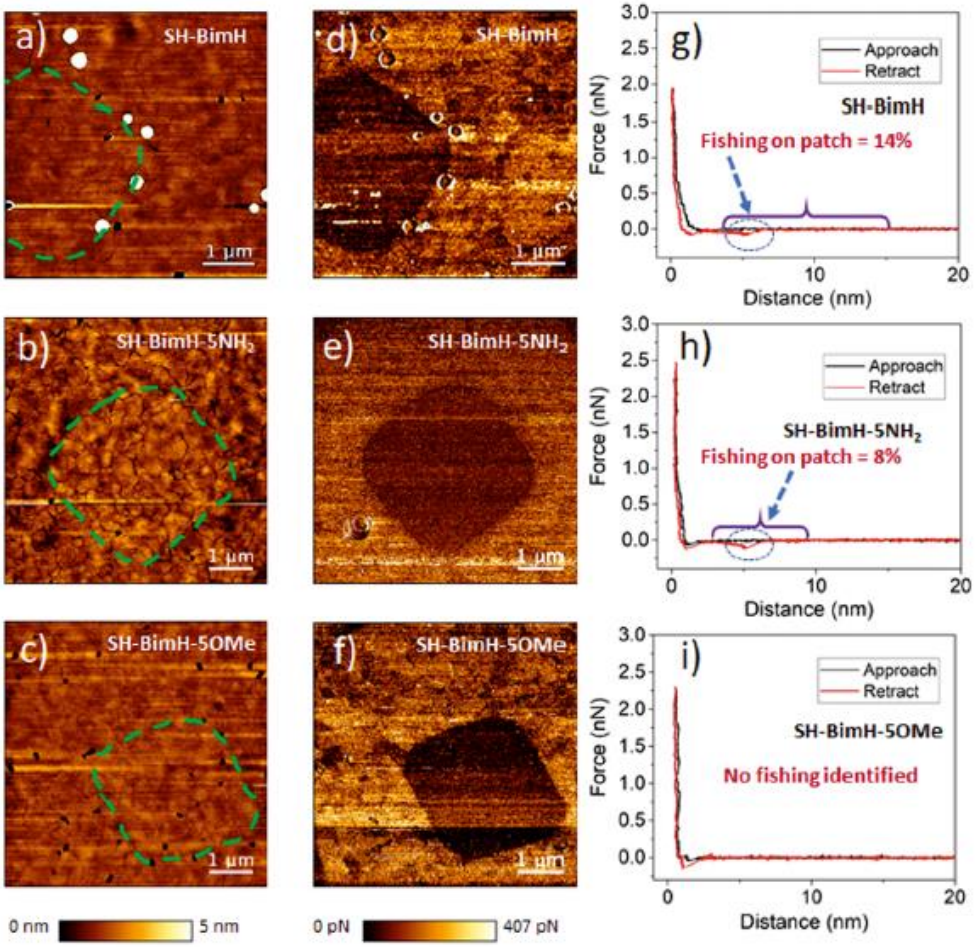

Figure 7. QI setpoint height images of Au surfaces printed with SH-BimH (a), SH-BimH-5NH_2 (b), and SH-BimH-5OMe (c). Adhesion images (d-f) corresponding to each inhibitor-modified surface, and FS curves (g-i) selected from the curves taken on each patch. For SH-BimH, 14% of the curves show "fishing" (g), for SH-BimH-5NH_2, 8% (h), and none for SH-BimH-5OMe (i).

Figure 7g-i presents the FS plots selected from the 'on patch' curves. Figure 7g,h shows typical examples which display a second peak in the retract curves. As mentioned previously, such additional peaks are caused by 'fishing' of molecules. This behavior was observed in

14% of the analyzed curves for the SH-BimH-patterned area and in the 8% of the analyzed curves for SH-BimH-5NH_2 patch. Furthermore, a variation of fishing distances was identified in the mentioned curves, which suggests that a group of molecules was pulled off from the surface. For the SH-BimH-printed surface, fishing phenomena were found in a (rather broad) distance range of about 5-15 nm as it is indicated in Figure 7g, whereas these phenomena in the SH-BimH-5NH_2 printed surface were identified at an also rather broad variation of distances of about 3-9 nm, as evidenced in Figure 7h. In contrast, the curve selected in the case of the printed surface with SH-BimH-5OMe observed in Figure 7i does not present any additional peak in its retract curve since no fishing event was identified in the data analysis, and, therefore, we assume a higher stability of the formed SAM. This argument agrees with previous FS studies, where SH-BimH-5OMe has been found to be the most stable molecule on Cu surfaces, compared to SH-BimH-5NH_2. Higher molecular stability was also correlated to enhanced corrosion efficiency, where the former molecule showed a better protective effect[27].

Derived from the variation of fishing distances previously observed, Figure 8 shows the schematic representations of two different possible fishing events. The short distances could indicate the fishing of a small number of molecules (Figure 8a), yet the necessary cohesive intermolecular forces may be too low as polymerization reactions are unlikely. Figure 8b, on the other hand, suggests the fishing of an accumulated layer, that is, sheet or “agglomerate” or “drop” of molecules. The latter is the more likely scenario as mostly distances of more than 3 nm are observed and where overall larger intermolecular van der Waals forces as well as hydrophobic forces in the water-based test solution might play a role. As a final remark, it would be expected that some of the molecules eventually reintroduce on the film during the subsequent force curve.

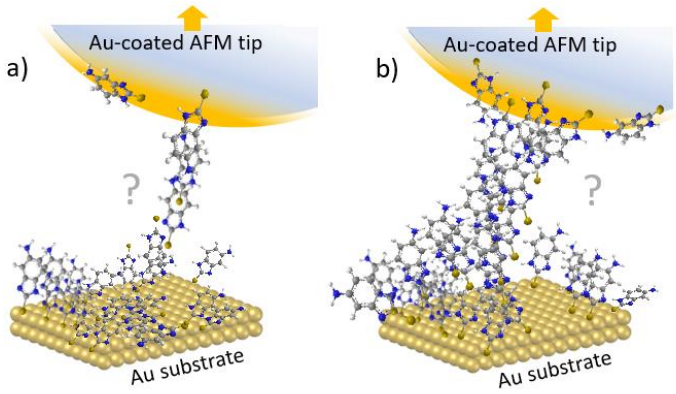

Figure 8. Schematic of fishing phenomena. Possible behavior for the fishing cases observed for SH-BimH-5NH_2 molecules. (a) Fishing of a chain of molecules and (b) fishing of a part of a layer.

Statistical analysis of adhesion curves and the results are displayed in Figure 9. FS measurements were carried out on homogeneously covered ultraflat Au surfaces in order to compare their nanomechanical properties with patterned surfaces. The adhesion values displayed in Figure 9a are obtained from the averaging over at least 100 retract curves for each type of surface. For the SAM-modified surfaces, the adhesion values are significantly reduced as compared to bare Au, owing to the presence of the corrosion inhibitors SAMs and, thus, the weaker interaction between the Au tip and the SAM layer. A close inspection of Figure 9a reveals a subtle difference in adhesion force between patterned and homogeneously covered surfaces. The latter displays larger adhesion force values for all three types of inhibitors as compared to the patterned, 'on patch' areas. The increased adhesion indicates that homogeneously applied (immersed) SAM layers are more disordered on average, and the force to detach the tip increases as a result of the close approach of the tip to the Au substrate, where an increase of contacts between the tip and the SAM layer is expected. In turn, patterned molecules form a more compact SAM layer and exhibit an enhanced stability as compared to the ones adsorbed directly from solution; hence, the distance and the number of possible tip-molecules contacts is reduced.

A similar argument has been utilized in the literature to assess the degree of order of supported lipid bilayers, for which an increase in the fluidity (disorder) of the bilayer induces a higher adhesion, as observed bilayers in the presence of nanoparticles[48] or anesthetics[49] . The enhanced stability of patterned SAMs agrees well with XPS results.

Figure 9b,c shows a detailed statistical analysis of adhesion forces for microcontact-printed surfaces on patch and out-of-patch locations (histograms for the remaining molecules are available in Figures S4 and S5 for homogeneously covered surfaces). Interestingly, out-of-patch locations which are supposed to be SAM-free display very small adhesion values as compared to bare Au. These small adhesion values could be the result of tip contamination, that is, displacement of molecules upon retraction of the tip, or possible diffusion of molecules upon exposure to water. The presence of a low number of molecules, either at the step edges or at the tip, can thus, from a nanomechanical point of view, have an influence. Earlier studies related to corrosion have evidenced influences of molecules in (bare) areas around printed patches[21]. The μ-cp technique was used to create heterogeneous SAM films as a method for studying dealloying (Figure S6)[20,21].

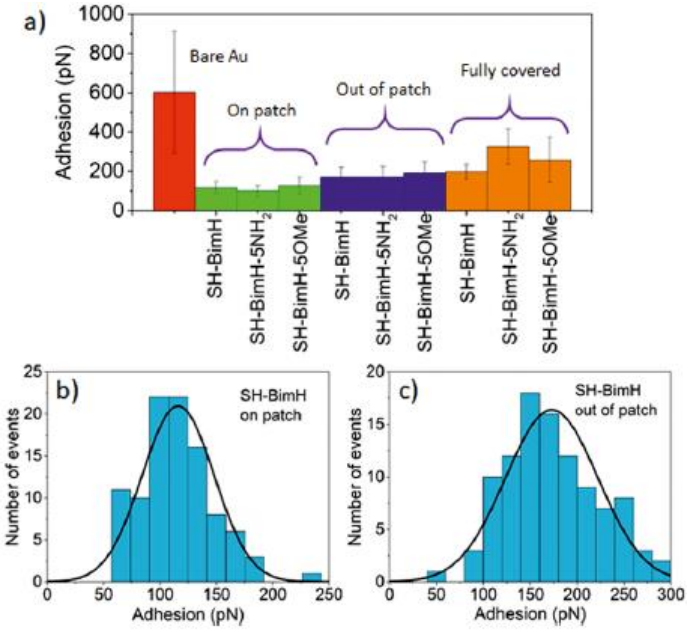

Figure 9. (a) Summary of average adhesion forces obtained from the selected FS curves on (left to right) bare Au, on patch, out-of-patch and immersed, fully covered surfaces. Adhesion histograms corresponding to the analyzed data obtained from FS measurements on μ-cp patterned ultraflat Au substrate with SH-BimH-5OMe (b) on patch and (c) out of patch.

Conclusions

The stability of microcontact-printed mercaptobenzimidazole-based corrosion inhibitor molecules on Au surfaces was assessed and compared to homogeneously covered films by means of a combination of surface-sensitive AFM and XPS techniques. Despite their rather compact chemical structures, we have shown the capability of these molecules to be microcontact printed on ultraflat Au surfaces, as evidenced from topographical AFM and chemical XPS signatures. XPS results show a strong covalent S-Au bonding, indicating the presence of well-ordered molecular films in both printed and homogeneous films, the former displaying a higher degree of order.

Nanomechanical AFM measurements confirmed the use of adhesion curves as useful descriptors for molecular stability to be further related with macroscopic properties. In particular, as compared to amino- and mercaptobenzimidazole analogues, a superior stability of self-assembled monolayers of methoxy-terminated SH-BimH-5OMe molecules was shown, as deduced from the absence of molecular fishing events upon tip retraction. Statistical analysis of adhesion forces has furthermore shown that microcontact-printed monolayers display a better stability than their counterparts formed by immersion, in agreement with XPS observations. The bare metal areas in between the print patches display smaller adhesion than bare Au, which might indicate molecules at the tip or that the printing process leaves some molecules outside the printed areas. With our demonstration of successful printing of real corrosion inhibitor molecules, our study calls for further steps toward fundamental understanding of more complex strategies involving corrosion inhibition.

Supporting Information

Characterization data including AFM; XPS spectra and adhesion histograms obtained from AFM-FS data analysis for all the analyzed samples; and figure related to the advantages of μ-cp in dealloying protection.

Acknowledgments

Financial support by FWO Odysseus program under G0D0115N project and FWO M.ERA-NET COINDESC project are greatly appreciated. We also acknowledge FWO for funding the HAXPES Lab instrument within the HERCULES program for Large Research Infrastructure of the Flemish government.

References

(1) Casalini, S.; Bortolotti, C. A.; Leonardi, F.; Biscarini, F. Self-Assembled Monolayers in Organic Electronics. *Chem. Soc. Rev.* **2017**, *46* (1), 40–71.

(2) Chaki, N. K.; Vijayamohanan, K. Self-Assembled Monolayers as a Tunable Platform for Biosensor Applications. *Biosens. Bioelectron.* **2002**, *17* (1–2), 1–12.

(3) MacChia, E.; Tiwari, A.; Manoli, K.; Holzer, B.; Ditaranto, N.; Picca, R. A.; Cioffi, N.; Di Franco, C.; Scamarcio, G.; Palazzo, G.; Torsi, L. Label-Free and Selective Single-Molecule Bioelectronic Sensing with a Millimeter-Wide Self-Assembled Monolayer of Anti-Immunoglobulins. *Chem. Mater.* **2019**, *31* (17), 6476–6483.

(4) Kim, S. Y.; Cho, S. J.; Byeon, S. E.; He, X.; Yoon, H. J. Self-Assembled Monolayers as Interface Engineering Nanomaterials in Perovskite Solar Cells. *Adv. Energy Mater.* **2020**, *10* (44), 2002606.

(5) Kovačević, N.; Milošev, I.; Kokalj, A. The Roles of Mercapto, Benzene, and Methyl Groups in the Corrosion Inhibition of Imidazoles on Copper: II. Inhibitor-Copper Bonding. *Corros. Sci.* **2015**, *98*, 457–470.

(6) Wu, X.; Wiame, F.; Maurice, V.; Marcus, P. 2-Mercaptobenzimidazole Films Formed at Ultra-Low Pressure on Copper: Adsorption, Thermal Stability and Corrosion Inhibition Performance. *Appl. Surf. Sci.* **2020**, *527*.

(7) Milošev, I.; Kovačević, N.; Kovač, J.; Kokalj, A. The Roles of Mercapto, Benzene and Methyl Groups in the Corrosion Inhibition of Imidazoles on Copper: I. Experimental Characterization. *Corros. Sci.* **2015**.

(8) Kokalj, A.; Lozinšek, M.; Kapun, B.; Taheri, P.; Neupane, S.; Losada-Pérez, P.; Xie, C.; Stavber, S.; Crespo, D.; Renner, F. U.; Mol, A.; Milošev, I. Simplistic Correlations between Molecular Electronic Properties and Inhibition Efficiencies: Do They Really Exist? *Corros. Sci.* **2021**, *179*.

(9) Finšgar, M.; Kek Merl, D. An Electrochemical, Long-Term Immersion, and XPS Study of 2-Mercaptobenzothiazole as a Copper Corrosion Inhibitor in Chloride Solution. *Corros. Sci.* **2014**, *83*, 164–175.

(10) Jennings, G. K.; Laibinis, P. E. Self-Assembled Monolayers of Alkanethiols on Copper Provide Corrosion Resistance in Aqueous Environments. *Colloids Surfaces A Physicochem. Eng. Asp.* **1996**, *116* (1–2), 105–114.

(11) Vericat, C.; Vela, M. E.; Benitez, G.; Carro, P.; Salvarezza, R. C. Self-Assembled Monolayers of Thiols and Dithiols on Gold: New Challenges for a Well-Known System. *Chemical Society Reviews*. 2010.

(12) Guo, Q.; Li, F. Self-Assembled Alkanethiol Monolayers on Gold Surfaces: Resolving the Complex Structure at the Interface by STM. *Phys. Chem. Chem. Phys.* **2014**, *16* (36), 19074–19090.

(13) Love, J. C.; Estroff, L. A.; Kriebel, J. K.; Nuzzo, R. G.; Whitesides, G. M. Self-Assembled Monolayers of Thiolates on Metals as a Form of Nanotechnology. *Chem. Rev.* **2005**.

(14) Marcus, P. Surface Science Approach of Corrosion Phenomena. *Electrochimica Acta*. 1998, pp 109–118.

(15) Renner, F. U.; Ankah, G. N.; Bashir, A.; Ma, D.; Biedermann, P. U.; Shrestha, B. R.; Nellessen, M.; Khorashadizadeh, A.; Losada-Pérez, P.; Duarte, M. J.; Raabe, D.; Valtiner, M. Star-Shaped Crystallographic Cracking of Localized Nanoporous Defects. *Adv. Mater.* **2015**, *27* (33), 4877–4882.

(16) Pareek, A.; Borodin, S.; Bashir, A.; Ankah, G. N.; Keil, P.; Eckstein, G. A.; Rohwerder, M.; Stratmann, M.; Gründer, Y.; Renner, F. U. Initiation and Inhibition of Dealloying of Single Crystalline Cu 3Au (111) Surfaces. *J. Am. Chem. Soc.* **2011**.

(17) Renner, F. U.; Stierle, A.; Dosch, H.; Kolb, D. M.; Lee, T. L.; Zegenhagen, J. Initial Corrosion Observed on the Atomic Scale. *Nature* **2006**, *439* (7077), 707–710.

(18) Maurice, V.; Marcus, P. Progress in Corrosion Science at Atomic and Nanometric Scales. *Progress in Materials Science*. Elsevier Ltd June 1, 2018, pp 132–171.

(19) Ankah, G. N.; Pareek, A.; Cherevko, S.; Zegenhagen, J.; Renner, F. U. Hierarchical Nanoporous Films Obtained by Surface Cracking on Cu-Au and Ethanethiol on Au(001). *Electrochim. Acta* **2014**, *140*, 352–358.

(20) Shrestha, B. R.; Bashir, A.; Ankah, G. N.; Valtiner, M.; Renner, F. U. Localized Dealloying Corrosion Mediated by Self-Assembled Monolayers Used as an Inhibitor System. *Faraday Discuss.* **2015**.

(21) Neupane, S.; Rivas, N. A.; Losada-Pérez, P.; D'Haen, J.; Noei, H.; Keller, T. F.; Stierle, A.; Rudolph, M.; Terfort, A.; Bertran, O.; Crespo, D.; Kokalj, A.; Renner, F. U. A Model Study on Controlling Dealloying Corrosion Attack by Lateral Modification of Surfactant Inhibitors. *npj Mater. Degrad. 2021 51* **2021**, *5* (1), 1–6.

(22) Perl, A.; Reinhoudt, D. N.; Huskens, J. Microcontact Printing: Limitations and Achievements. *Adv. Mater.* **2009**, *21* (22), 2257–2268.

(23) Smith, R. K.; Lewis, P. A.; Weiss, P. S. Patterning Self-Assembled Monolayers. *Prog. Surf. Sci.* **2004**, *75* (1–2), 1–68.

(24) Neupane, S.; Losada-Pérez, P.; Vivegnis, S.; Mekhalif, Z.; Delhalle, J.; Bashir, A.; Renner, F. U. Two-Step Nanoscale Approach for Well-Defined Complex Alkanethiol Films on Au Surfaces. *Langmuir* **2018**.

(25) Doneux, T.; Buess-Herman, C.; Lipkowski, J. Electrochemical and FTIR Characterization of the Self-Assembled Monolayer of 2-Mercaptobenzimidazole on Au(1 1 1). *J. Electroanal. Chem.* **2004**, *564* (1–2), 65–75.

(26) Doneux, T.; Buess-Herman, C.; Hosseini, M. G.; Nichols, R. J.; Lipkowski, J. Adsorption of 2-Mercaptobenzimidazole on a Au(1 1 1) Electrode. *Electrochim. Acta* **2005**, *50* (21), 4275–4282.

(27) Neupane, S.; Losada-Pérez, P.; Tiringer, U.; Taheri, P.; Desta, D.; Xie, C.; Crespo, D.; Mol, A.; Milošev, I.; Kokalj, A.; Renner, F. U. Study Of Mercaptobenzimidazoles As Inhibitors For Copper Corrosion: Down to the Molecular Scale. *J. Electrochem. Soc.* **2021**, *168* (5), 051504.

(28) Oncins, G.; Vericat, C.; Sanz, F. Mechanical Properties of Alkanethiol Monolayers Studied by Force Spectroscopy. *J. Chem. Phys.* **2008**, *128* (4).

(29) Dicke, C.; Hähner, G. Interaction between a Hydrophobic Probe and Tri(Ethylene Glycol)-Containing Self-Assembled Monolayers on Gold Studied with Force Spectroscopy in Aqueous Electrolyte Solution. *J. Phys. Chem. B* **2002**, *106* (17), 4450–4456.

(30) Akimoto, K.; Sato, F.; Morikawa, T.; Fujihira, M. Effects of Chain Length on Adhesive Force between Gold Tip and Gold Substrate Covered with Alkanethiol Self-Assembled Monolayers. *Japanese J. Appl. Physics, Part 1 Regul. Pap. Short Notes Rev. Pap.* **2004**, *43* (7 B), 4492–4498.

(31) Caballero, D.; Pla-Roca, M.; Bessueille, F.; Mills, C. A.; Samitier, J.; Errachid, A. Atomic Force Microscopy Characterization of a Microcontact Printed, Self-Assembled Thiol Monolayer for Use in Biosensors. **2007**, *39* (8), 1721–1734.

(32) Finšgar, M. 2-Mercaptobenzimidazole as a Copper Corrosion Inhibitor: Part II. Surface Analysis Using X-Ray Photoelectron Spectroscopy. *Corros. Sci.* **2013**, *72*, 90–98.

(33) Xue, G.; Huang, X. Y.; Dong, J.; Zhang, J. The Formation of an Effective Anti-Corrosion Film on Copper Surfaces from 2-Mercaptobenzimidazole Solution. *J. Electroanal. Chem.* **1991**, *310* (1–2), 139–148.

(34) Hale, P. S.; Kappen, P.; Prissanaroon, W.; Brack, N.; Pigram, P. J.; Liesegang, J. Minimizing Silicone Transfer during Micro-Contact Printing. *Appl. Surf. Sci.* **2007**, *253* (8), 3746–3750.

(35) Jain, A.; Bharadwaj, P.; Heeg, S.; Parzefall, M.; Taniguchi, T.; Watanabe, K.; Novotny, L. Minimizing Residues and Strain in 2D Materials Transferred from

PDMS. *Nanotechnology* **2018**, *29* (26), 265203.

(36) Thibault, C.; Séverac, C.; Mingotaud, A. F.; Vieu, C.; Mauzac, M. Poly(Dimethylsiloxane) Contamination in Microcontact Printing and Its Influence on Patterning Oligonucleotides. *Langmuir* **2007**, *23* (21), 10706–10714.

(37) Foley, J. O.; Fu, E.; Gamble, L. J.; Yager, P. Microcontact Printed Antibodies on Gold Surfaces: Function, Uniformity, and Silicone Contamination. *Langmuir* **2008**, *24* (7), 3628–3635.

(38) Xue, C. Y.; Chin, S. Y.; Khan, S. A.; Yang, K. L. UV-Defined Flat PDMS Stamps Suitable for Microcontact Printing. *Langmuir* **2010**, *26* (5), 3739–3743.

(39) Glasmästar, K.; Gold, J.; Andersson, A. S.; Sutherland, D. S.; Kasemo, B. Silicone Transfer during Microcontact Printing. *Langmuir* **2003**, *19* (13), 5475–5483.

(40) Yunus, S.; De Crombrugghe De Looringhe, C.; Poleunis, C.; Delcorte, A. Diffusion of Oligomers from Polydimethylsiloxane Stamps in Microcontact Printing: Surface Analysis and Possible Application. *Surf. Interface Anal.* **2007**, *39* (12–13), 922–925.

(41) Whelan, C. M.; Smyth, M. R.; Barnes, C. J.; Brown, N. M. D.; Anderson, C. A. An XPS Study of Heterocyclic Thiol Self-Assembly on Au(111). *Appl. Surf. Sci.* **1998**, *134* (1–4), 144–158.

(42) Deng, X.; Sorescu, D. C.; Lee, J. Single-Layer ZnS Supported on Au(111): A Combined XPS, LEED, STM and DFT Study. *Surf. Sci.* **2017**, *658*, 9–14.

(43) Gichuhi, A.; Shannon, C.; Perry, S. S. A Scanning Tunneling Microscopy and X-Ray Photoelectron Spectroscopy Study of Electrochemically Grown ZnS Monolayers on Au(111). *Langmuir* **1999**, *15* (17), 5654–5661.

(44) Butt, H. J.; Cappella, B.; Kappl, M. Force Measurements with the Atomic Force Microscope: Technique, Interpretation and Applications. *Surf. Sci. Rep.* **2005**, *59* (1–6), 1–152.

(45) Neupane, K.; Zhao, M.; Lyons, A.; Munshi, S.; Ileperuma, S. M.; Ritchie, D. B.; Hoffer, N. Q.; Narayan, A.; Woodside, M. T. Structural Dynamics of Single SARS-

CoV-2 Pseudoknot Molecules Reveal Topologically Distinct Conformers. *Nat. Commun. 2021 121* **2021**, *12* (1), 1–9.

(46) Arbore, C.; Perego, L.; Sergides, M.; Capitanio, M. Probing Force in Living Cells with Optical Tweezers: From Single-Molecule Mechanics to Cell Mechanotransduction. *Biophys. Rev.* **2019**, *11* (5), 765–782.

(47) Mandal, S. S. Force Spectroscopy on Single Molecules of Life. *ACS Omega* **2020**, *5* (20), 11271–11278.

(48) Bar, L.; Perissinotto, F.; Redondo-Morata, L.; Giannotti, M. I.; Goole, J.; Losada-Pérez, P. Interactions of Hydrophilic Quantum Dots with Defect-Free and Defect Containing Supported Lipid Membranes. *Colloids Surfaces B Biointerfaces* **2022**, *210*, 112239.

(49) Leonenko, Z.; Finot, E.; Cramb, D. AFM Study of Interaction Forces in Supported Planar DPPC Bilayers in the Presence of General Anesthetic Halothane. *Biochim. Biophys. Acta - Biomembr.* **2006**, *1758* (4), 487–492.

Table of contents graphic

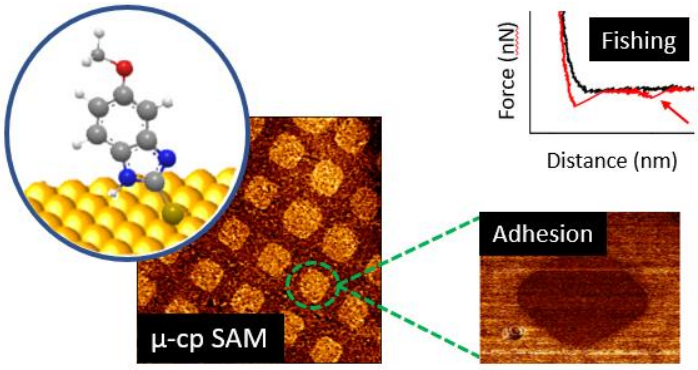

Supporting information

Nanomechanical stability of laterally heterogeneous films of corrosion inhibitor molecules obtained by microcontact printing on Au model substrates

Andrea Valencia Ramirez[a,b], Gilles Bonneux[a,b], Andreas Terfort[c], Patricia Losada-Pérez[d], Frank Uwe Renner[a,b*]

[a] Institute for Materials Research, Hasselt University, 3590 Diepenbeek, Belgium

[b] IMEC, Division IMOMEC, 3590 Diepenbeek, Belgium

[c] Institute of Inorganic and Analytical Chemistry, Goethe-University, 60438 Frankfurt am Main, Germany

[d] Experimental Soft Matter and Thermal Physics Laboratory, Université Libre de Bruxelles (ULB), 1050 Brussels, Belgium

*Email: frank.renner@uhasselt.be

Here we present the supporting information for our manuscript where we analyze the self-assembly behavior of organic molecules with potential application as corrosion inhibitors. These molecules were patterned on ultraflat Au surfaces using microcontact printing and characterized using Atomic Force Microscopy (AFM), X ray Photoelectron Spectroscopy (XPS) and AFM force spectroscopy (AFM-FS) with a quantitative imaging mode (QI). It was observed a superior nanomechanical stability as well as a high ordering degree of the SAMs formed by microcontact printing compared to homogeneously inhibitor covered Au surfaces.

The present document shows information corresponding to the analyzed data of all the inhibitors used in the study, as well as a remark regarding silicone traces identified from the polydimethylsiloxane (PDMS) stamp.

Contents

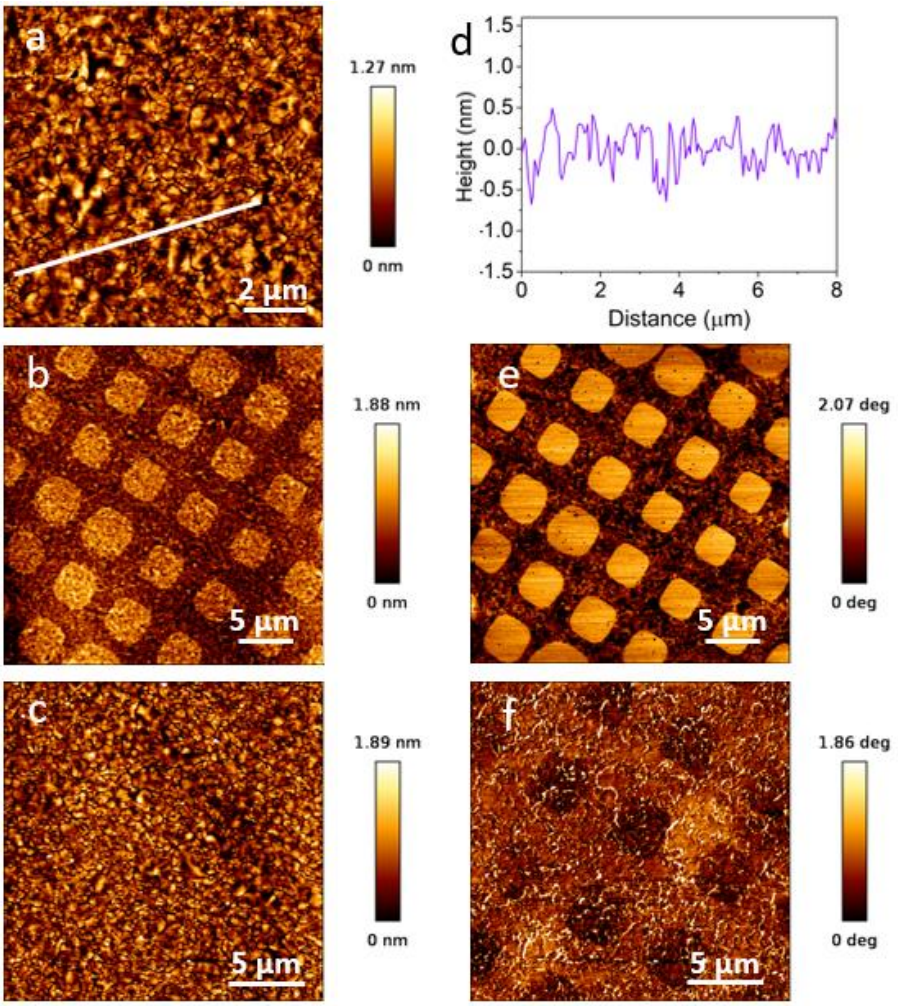

Figure S1. AFM height images of (a) bare ultraflat Au substrate (10 x 10 μm^2), (b) printed with SH-BimH, (c) printed with blank PDMS stamp, (d) height cross section profile of (a) and (e,f) AFM phase images of (b) and (c) respectively. It is noticed in (f) that traces of microcontact printing are present, presumably due to PDMS transfer from the stamp.

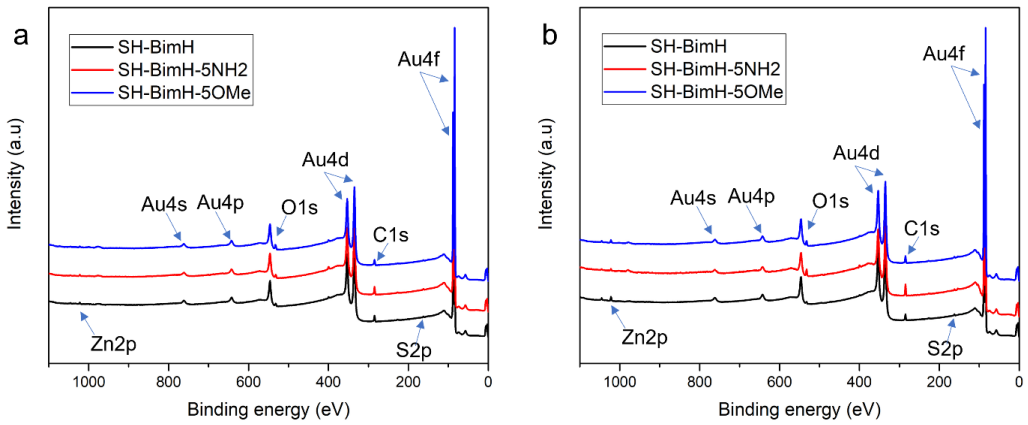

Figure S2. XPS spectra of (a) fully inhibitor covered and (b) microcontact printed ultraflat Au surfaces. Zn peaks are less noticed in figure (a) indicating the homogeneous surface coverage, whereas in (b) printed surfaces, Zn peaks still visible due to the hybrid formed films.

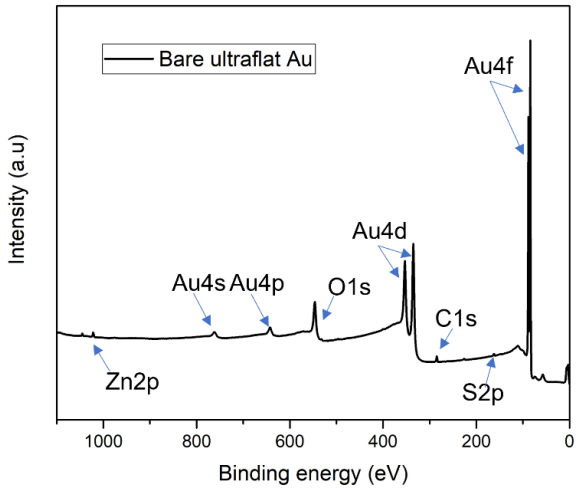

Figure S3. XPS spectra of a bare ultraflat Au surface. Zn presence is also detected thus we attribute it to the manufacturing process.

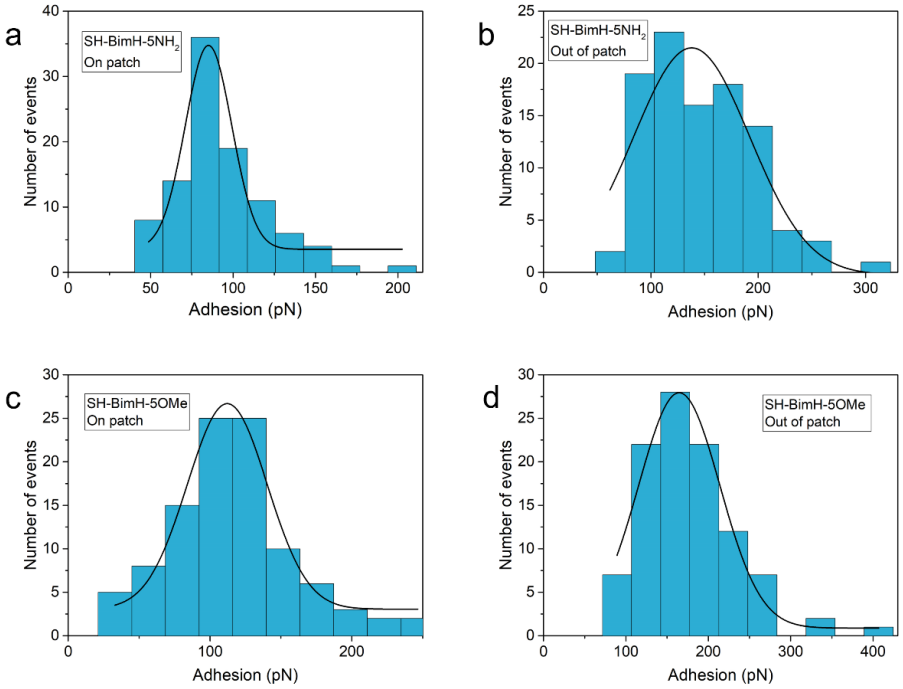

Figure S4. Adhesion histograms corresponding to the analyzed data obtained from force spectroscopy measurements on patterned ultraflat Au surfaces with SH-BimH-5NH_2 (a) on patch (b) out of patch and with SH-BimH-5OMe (c) on patch (d) out of patch.

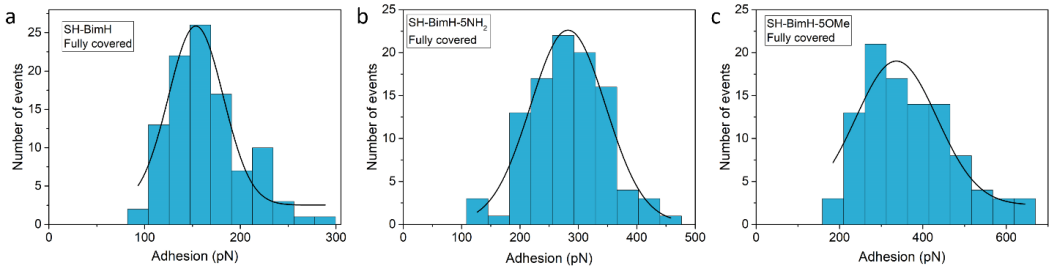

Figure S5. Adhesion histograms corresponding to the analyzed data obtained from force spectroscopy measurements on fully covered ultraflat Au surfaces with (a) SH-BimH, (b) SH-BimH-5NH_2 and (c) SH-BimH-5OMe. It is observed that these adhesion values are higher than on patterned surfaces in all the cases.

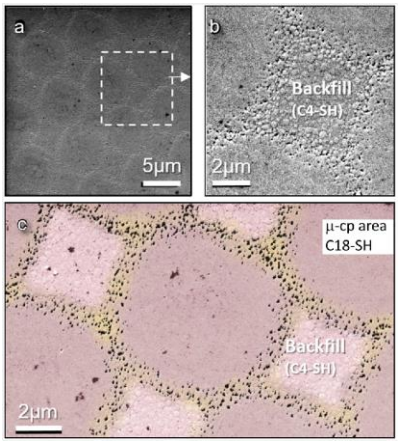

Figure S6. Localized initial dealloying along artificial SAM patch boundaries created by µCP and backfilling. (a) SEM image of µCP-C_{18}-SH/C_4-SH modified atomically-flat surface after dealloying. (b) Zoom-in to initial dealloying region, contrast-enhanced SEM image. (c) Color-modified SEM image showing localized initial dealloying along artificial SAM boundaries[1].

Reproduced with permission from Neupane et al., npj Materials Degradation (2021) 5:29; https://doi.org/10.1038/s41529-021-00169-2

References

1. Neupane, S.; Rivas, N. A.; Losada-Pérez, P.; D'Haen, J.; Noei, H.; Keller, T. F.; Stierle, A.; Rudolph, M.; Terfort, A.; Bertran, O.; Crespo, D.; Kokalj, A.; Renner, F. U. A Model Study on Controlling Dealloying Corrosion Attack by Lateral Modification of Surfactant Inhibitors. *npj Mater. Degrad.* **2021**, *5*, 1–6.